possible to close system (3-7) and to perform thermohydraulic calculations for heat exchangers for the above-examined type of transience.

NOTATION

N, Power of thermal load; τ, time; G_1, initial flow rate of heat carrier; G_2, maximum flow rate of heat carrier after introduction of a perturbation into the feed system; m, porosity of the bundle with respect to the heat carrier; K, dimensionless effective diffusion coefficient; D_t, effective diffusion coefficient; u, v, longitudinal and radial velocities; d_e, equivalent diameter of the bundle; Fr_m, criterion characterizing the intensity of swirling of the flow in the bundle of coiled tubes; S, pitch of the tube coiling; d, maximum dimension of tube profile; Fo_b, Fourier criterion; d_{bu}, r_{bu}, diameter and radius of the tube bundle; λ, thermal conductivity; c_p, heat capacity; ρ, density; ξ, hydraulic resistance coefficient; γ, kinematic viscosity; $\varkappa$, relative diffusion coefficient; T, temperature; x, r, longitudinal and radial coordinates. Indices: b, mean-mass; w, wall; n, nonsteady; qs, quasi-steady; m, maximum; e, effective; s, solid phase.

LITERATURE CITED

1. Yu. I. Danilov, B. V. Dzyubenko, G. A. Dreitser, and L. A. Ashmantas, Heat Transfer and Hydrodynamics in Channels of Complex Form [in Russian], Moscow (1986).
2. B. V. Dzyubenko, M. D. Segal', L. A. Ashmantas, and P. A. Urbonas, Izv. Akad. Nauk SSSR, Énerg. Transp., No. 3, 125-133 (1983).
3. B. V. Dzyubenko, L. A. Ashmantas, M. D. Segal', and P. A. Urbonas, Izv. Akad. Nauk SSSR, Énerg. Transp., No. 4, 110-118 (1985).
4. B. V. Dzyubenko, L. A. Ashmantas, and A. B. Bagdonavichyus, Inter-Institute Collection of Scientific Transactions: Current Problems of Hydrodynamics and Heat Transfer in Elements of Power Plants and Cryogenic Technology, Vol. 14, 9-14, Moscow (1985).
5. B. V. Dzyubenko, L. A. Ashmantas, A. B. Bagdonavichyus, and M. D. Segal', Inzh.-Fiz. Zh., 54, No. 4, 533-539 (1988).
6. L. A. Ashmantas, B. V. Dzyubenko, G. A. Dreitser, and M. D. Segal, Int. J. Heat Mass Transfer, 28, No. 4, 867-877 (1985).
7. B. V. Dzyubenko, L. A. Ashmantas, and A. B. Bagdonavichyus, Inzh.-Fiz. Zh., 55, No. 3, 357-363 (1988).
8. É. K. Kalinin, G. A. Dreitser, V. V. Kostyuk, and I. I. Berlin, Methods of Calculating Coupled Heat-Transfer Problems [in Russian], Moscow (1983).

STUDY OF HYDRODYNAMICS AND MASS TRANSFER IN THE FLOW OF OPPOSITELY SWIRLED JETS ABOUT A STABILIZER IN AN ANNULAR CHANNEL

K. Yu. Sokolov, A. G. Tumanovskii, A. I. Maiorova, A. V. Sudarev, and E. D. Vinogradov

UDC 532.517.4

Experimental and theoretical methods are used to study the distribution of the velocity components, turbulence intensity, and the concentration of a passive impurity. An analysis is made of the effect of the main geometric parameters on the intensity of transport processes.

At present in the annular combustion chambers of gas-turbine units, combustion takes place in a system of oppositely swirled jets of gaseous and liquid fuel [1].

The results of experimental [1, 2] and theoretical [2] studies of the separation zone after the stabilizer and the available data on the displacement of oppositely swirled jets in an annular channel [3, 4] prove to be inadequate to analyze processes taking place in the

F. É. Dzerzhinskii All-Union Scientific-Research Institute of Heat Engineering, Moscow.

Translated from Inzhenerno-Fizicheskii Zhurnal, Vol. 56, No. 1, pp. 12-18, January, 1988. Original article submitted August 10, 1987.

0022-0841/89/5601-0006 $12.50

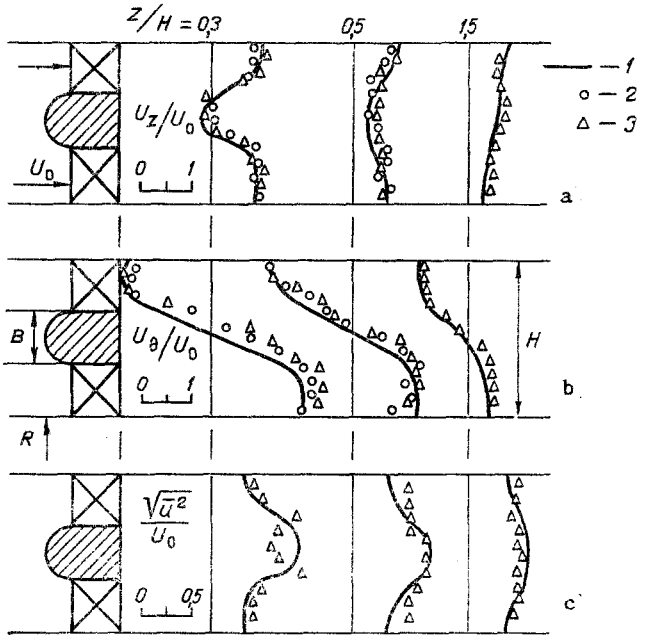

Fig. 1. Change in the axial (a) and tangential (b) components of velocity and turbulence intensity (c) along the channel for the opposite-swirling variant ±60°: 1) calculation; 2, 3) experiment: 2) head meter; 3) hot-wire anemometer.

frontal zone. Additional theoretical and experimental studies of turbulent flow and mass transfer are needed. The results of such studies are reported below.

1. Measurements were made on a large-scale model of a combustion chamber. The model was in the form of an annular channel formed by two coaxial cylinders with diameters of 780 and 1220 mm.

Vane swirlers were installed in the channel inlet. The swirlers were twisted in opposite directions and were separated by an annular stabilizer with a blunt end surface which was perforated to admit natural gas (Fig. 1).

We studied different angles of opposite swirling of the jets: ±60°; ±45°; 0°. The degree of obstruction of the channel $K_F = B/H$ (B is the height of the stabilizer; H is the height of the channel) was 0.35. The axial (U_Z) and tangential (U_θ) components of velocity were measured with a spherical five-channel head meter with a ball 5 mm in diameter.

To determine turbulence intensity and to check and enhance the accuracy of measurements of the velocity components U_Z and U_θ, we used a hot-wire anemometer having a miniature sensitive element with a single tungsten wire 2 mm long and 3 μm in diameter. The methodology was described in detail in [5]. The errors of measurement of the velocity components with the head meter were 5% outside the recirculation zone and as high as 40% inside the zone. The error of the anemometric measurements in turbulent swirled flows with a high turbulence intensity was examined in [4, 6], where it was estimated to be 15-20% for the mean velocity components and 25-35% for the fluctuation components.

To determine the rate of mass transfer in the frontal zone, we fed a passive impurity, methane, through a perforation in the end surface of the stabilizer. The concentration field of the impurity was measured with a gas analyzer.

2. The theoretical study was conducted by numerically solving the system of equations describing steady-state turbulent motion for an axisymmetric flow with allowance for rotation [7]:

$$\frac{\partial U_z}{\partial z} + \frac{1}{r}\frac{\partial}{\partial r} rU_r = 0; \tag{1}$$

$$\frac{\partial U_z^2}{\partial z} + \frac{1}{r}\frac{\partial}{\partial r} rU_rU_z = -\frac{1}{\rho}\frac{\partial P}{\partial z} + 2\frac{\partial}{\partial z}(\nu_t + \nu)\frac{\partial U_z}{\partial z} + \frac{1}{r}\frac{\partial}{\partial r}\left(r(\nu_t + \nu)\left(\frac{\partial U_z}{\partial r} + \frac{\partial U_r}{\partial z}\right)\right); \tag{2}$$

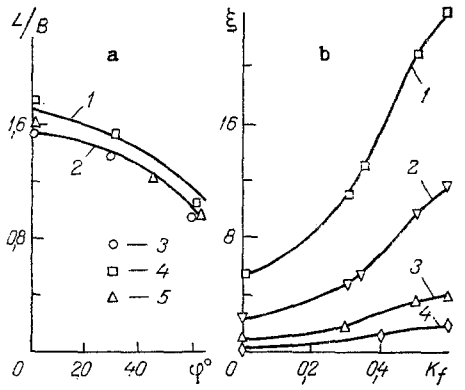

Fig. 2

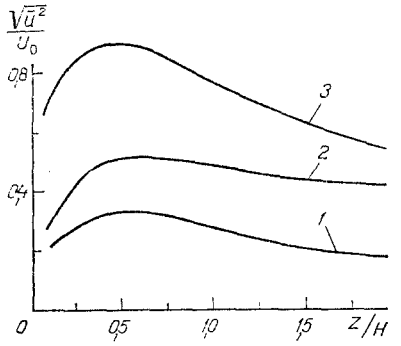

Fig. 3

Fig. 2. Dependence of the flow characteristics on the angle of opposite swirl and the degree of obstruction of the channel: a) length of separation zone; 1, 2) calculation (1– K_F = 0.45; 2 – 0.35); 3, 5) experiment [2]; (K_F = 0.29 and 0.42); 4) present experiment (K_F = 0.35); b) total pressure loss coefficient: 1) $\phi = \pm 60°$; 2) $\pm 45°$; 3) $\pm 30°$; 4) $\pm 20°$.

Fig. 3. Change of turbulence intensity maximum in the cross section along the channel (K_F = 0.35): 1) $\phi = \pm 60°$; 2) $\pm 45°$; 3) 0°.

$$\frac{\partial}{\partial z}U_zU_r+\frac{1}{r}\frac{\partial}{\partial r}rU_r^2=-\frac{1}{\rho}\frac{\partial P}{\partial r}+\frac{\partial}{\partial z}\left((\nu_t+\nu)\left(\frac{\partial U_z}{\partial r}+\frac{\partial U_r}{\partial z}\right)\right)+$$
$$+\frac{2}{r}\frac{\partial}{\partial r}r(\nu_t+\nu)\frac{\partial U_r}{\partial r}-2(\nu_t+\nu)\frac{U_r}{r^2}+\frac{U_\theta^2}{r}; \qquad (3)$$

$$\frac{\partial}{\partial z}U_rrU_\theta+\frac{1}{r}\frac{\partial}{\partial r}r^2U_rU_\theta=\frac{\partial}{\partial z}(\nu_t+\nu)\frac{\partial rU_\theta}{\partial z}+\frac{1}{r}\frac{\partial}{\partial r}r(\nu_t+\nu)\frac{\partial rU_\theta}{\partial r}-\frac{2}{r}\frac{\partial}{\partial r}(\nu_t+\nu)U_\theta r. \qquad (4)$$

To determine ν_t, we use an improved two-parameter model of turbulence k – W [8] (k is the kinetic turbulence energy and W is "pseudovorticity"); $\nu_t = k/\sqrt{W}$;

$$\frac{\partial U_zk}{\partial z}+\frac{1}{r}\frac{\partial}{\partial r}U_rrk=\frac{\partial}{\partial z}\left(\frac{\nu_t}{\sigma_K}+\nu\right)\frac{\partial k}{\partial z}+\frac{1}{r}\frac{\partial}{\partial r}r\left(\frac{\nu_t}{\sigma_K}+\nu\right)\frac{\partial k}{\partial r}+S_K, \qquad (5)$$

$$\frac{\partial U_zW}{\partial z}+\frac{1}{r}\frac{\partial}{\partial r}U_rrW=\frac{\partial}{\partial z}\left(\frac{\nu_t}{\sigma_W}+\nu\right)\frac{\partial W}{\partial z}+\frac{1}{r}\frac{\partial}{\partial r}r\left(\frac{\nu_t}{\sigma_W}+\nu\right)\frac{\partial W}{\partial r}+S_W. \qquad (6)$$

Here, S_K and S_W are the source terms of the transport equations:

$$S_K=\nu_tF_K-C_Dk\sqrt{W}, \qquad (7)$$

$$S_W=C_{1W}\nu_t\left(\left(\frac{\partial\omega}{\partial z}\right)^2+\left(\frac{\partial\omega}{\partial r}\right)^2+\left(\frac{\omega}{r}\right)^2\right)-C_{2W}(1-C_R\mathrm{Ri})W^{3/2}+C_{3W}\frac{W}{k}\nu_tF_K+C_{4W}W^{3/2}\left(\mathrm{grad}\sqrt{\frac{k}{W}}\right)^2 \qquad (8)$$

$$F_K=2\left(\left(\frac{\partial U_z}{\partial z}\right)^2+\left(\frac{\partial U_r}{\partial r}\right)^2+\left(\frac{U_r}{r}\right)^2\right)+\left(\frac{\partial U_\theta}{\partial z}\right)^2+\left(r\frac{\partial}{\partial r}\frac{U_\theta}{r}\right)^2+\left(\frac{\partial U_z}{\partial r}+\frac{\partial U_r}{\partial z}\right)^2, \qquad (9)$$

$$\mathrm{Ri}=\frac{2\frac{U_\theta}{r^2}\frac{\partial}{\partial r}rU_\theta}{\left(\frac{\partial U_z}{\partial r}\right)^2+\left(r\frac{\partial}{\partial r}\frac{U_\theta}{r}\right)^2}\quad\text{Richardson number.}$$

The introduction of an additional term containing the Richardson number into the source term S_W in a first approximation allows us to consider enisotropy of eddy viscosity associated with the curvature of the streamlines on the spatial scale of turbulence C_D = 0.09; C_{1W} =

3.5; $C_{2W} = 0.17$; $C_{3W} = 1.04$; $C_{4W} = 2.97$: $\sigma_K = \sigma_W = 0.9$ are constants of the model [8]. The value of C_R was taken equal to 1, in accordance with [9].

In solving Eqs. (1)-(6), we excluded pressure from them by introducing new variables, the stream function ψ and vorticity function ω, so that

$$U_z = \frac{1}{r}\frac{\partial \psi}{\partial r};\ U_r = -\frac{1}{r}\frac{\partial \psi}{\partial z};\ \omega = \frac{\partial U_r}{\partial z} - \frac{\partial U_z}{\partial r}. \tag{10}$$

We then used a "hybrid" finite-difference method [10].

We assigned values of the stream function as boundary conditions for the impermeable walls. For the remaining variables, the boundary conditions were assigned one grid spacing deeper into the flow, where we assumed that the universal logarithmic "wall law" for total velocity was satisfied [7]:

$$\frac{\sqrt{U_z^2 + U_\theta^2}}{u^*} = \frac{1}{\varkappa}\ln\frac{u^* h}{\nu} + A;\ k = \frac{u^{*2}}{\sqrt{C_D}};\ W = \frac{u^{*2}}{\varkappa^2 h^2 C_D}. \tag{11}$$

Here $\varkappa = 0.41$; $A = 5.36$; u^* is dynamic velocity; h is the distance from the wall.

In the inlet section, located several grid spacings in front of the end surface, we assigned the profiles of ψ, ω, U_θ, k, and W; at the outlet, we assumed that the longitudinal derivatives of all of the dependent variables were equal to zero.

The logarithmic law was not adopted near points of inflection after the sudden expansion. Instead, we imposed the condition of convergence of the streamlines from the inflection point in the horizontal direction. We solved the corresponding differential equations (4) and (5) for the tangential component of velocity and turbulence energy near the point. Meanwhile, the flow through the left boundary of the control cell was calculated with allowance for the logarithmic layer, while we followed [11] in finding W by using the condition of proportionality of the turbulence scale in the mixing layer beyond the offset to the width of the layer [12], calculated with allowance for the swirling.

The distribution of the concentration of the passive impurity was determined by solving the transport equation

$$\frac{\partial U_z C}{\partial z} + \frac{1}{r}\frac{\partial r U_r C}{\partial r} = \frac{\partial}{\partial z}\left(\frac{\nu_t}{\sigma_C} + \nu\right)\frac{\partial C}{\partial z} - \frac{1}{r}\frac{\partial}{\partial r}\left(\frac{\nu_t}{\sigma_C} + \nu\right) r\frac{\partial C}{\partial r} = 0 \tag{12}$$

for a precalculated flow field. Here, the turbulent Schmidt number $\sigma_C = 0.9$. The concentration was assigned equal to unity along the front surface on the nearest layer of the difference grid. On all of the other solid boundaries, we assigned conditions of the form $\partial C/\partial n = 0$, where n is the normal to the surface; at the outlet, we assigned the condition $\partial C/\partial z = 0$.

The length of the calculated region was 3H. Calculations performed with refinement of the grid showed that a 31 × 36 grid is optimum. the calculations were performed on a BESM-6 computer.

3. Figure 1 shows calculated and experimental data on the profiles of axial and tangential velocity and turbulence intensity for the swirl variant ±60°. For all of the investigated variants, the velocity component profiles obtained in the calculations agree satisfactorily with the data from thermoanemometric and pneumometric measurements. As regards turbulence intensity, the scatter of the theoretical and experimental results is no more than 30%. This figure corresponds to the above-indicated accuracy of the measurements of the fluctuation component of velocity.

Figure 2 shows the dependence of the relative length of the separation zone L/B on the angle of installation of the swirlers for two degrees of obstruction 0.35 and 0.45. Here, experimental data from [2] is also shown for comparison.

It can be seen from the figure that an increase in the angles of opposite swirl is accompanied by a monotonic decrease in the relative length of the separation zone. As in the case of the flow of an unswirled jet past an offset in a channel [13], an increase in the degree of obstruction of the channel up to 0.55-0.6 leads to an increase in L/B for all variants of swirl angles. The value of L/B is maximal at a degree of blockage equal to 0.55-0.6.

The calculations showed that within the range $0.8 \leq R/H \leq 10$ (R is the radius of the internal cylinder), the radius of curvature of the annular channel does not have a significant

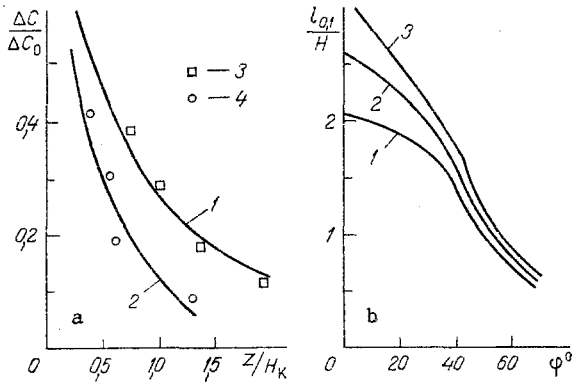

Fig. 4. Effect of the angle of twist and the degree of obstruction on the rate of mixing of a passive impurity: a) change in the relative nonuniformity of the concentration profile along the channel (K_F= 0.35); 1-2) calculation; 3-4) experiment; 1, 3) $\phi = \pm 60°$; 2, 4) $\phi = 0°$; b) dependence of the characteristic distance $\ell_{0,1}$ on the angle of swirl: 1) $K_F = 0.27$; 2) 0.35; 3) 0.55.

effect on the flow field in the recirculation region, given identical conditions at the inlet.

Figure 2b shows the dependence of the total pressure loss coefficient in the combustion chamber on the angle of installation of the swirl vanes and degree of blockage. This data was obtained experimentally. It shows that there is an increase in the total pressure loss coefficient with an increase in ϕ and K_F. This increase can be approximated by the expression

$$\xi = \frac{2\Delta P^*}{\rho U_0^2 (1 - K_F)} = \exp(-2{,}3K_F^2 + 4{,}37K_F + 4{,}92 \sin\varphi - 2{,}88). \quad (13)$$

4. It is of practical interest to study the effect of the main geometric parameters on the intensity of transport processes in the frontal zone.

As was done for submerged jets in [12] and oppositely swirled annular jets separated by a thin partition at the inlet in [3], for the flow being examined here we can establish a relationship between the intensity of transport processes for different swirl angles and the level of turbulence in the flow (or the maximum turbulence intensity, which reflects this level).

Figure 3 shows the calculated change in maximum turbulence intensity over the cross section along the channel fir different swirl angles. It can be seen that an increase in the degree of opposite swirling is accompanied by a rapid increase in turbulent pulsations.

In the absence of swirling, turbulence intensity increases only in the immediate vicinity of the end surface, due to the generation of turbulence energy in mixing layers formed near the edges of the stabilizer. Here, the distribution of turbulence intensity over the height of the channel has two distinct local maxima corresponding to these layers.

With large angles of opposite swirl ($\pm 60°$, $\pm 45°$), at the end of the recirculation zone there is an intensive increase in turbulence energy on the axis of the annular channel. This increase is due to displacement of the tangential velocity component. In this case, the profile of turbulence intensity has a single local maximum located at the center of the section.

Another characteristic of the intensity of transport processes is a criterion based on the degree of levelling, along the channel, of the concentration profile of a passive impurity introduced into the flow through the end surface of the stabilizer. Figure 4 shows the change in the relative nonuniformity of the concentration profile $\Delta C/\Delta C_0$ along the channel for different angles of swirl. The data shows that an increase in the angles of opposite swirl of the flows is accompanied by a reduction in the length of the section over which

mixing of the flows is achieved. Here, $\Delta C = C_{max} - C_{min}$ is the nonuniformity of the concentration profile in the given section and ΔC_0 is the same quantity at the inlet (in the calculation, on the layer of the difference grid closest to the end surface; in the experiment, in the first section $z/H = 0.2$).

The calculations show that an increase in the degree of obstruction of the channel also intensifies mixing along the channel. Thus, the distance over which the nonuniformity of the concentration profile decreases by a certain factor – such as 0.1 ($\ell_{0.1}$) – can be used as an index of the rate of mass transfer after the stabilizer.

The dependence of the characteristic distance $\ell_{0.1}$ on the angle of swirl and the degree of obstruction (Fig 4b) within the range $K_F = 0.25$-0.65; $\phi = 0$-$70°$ can be approximated by the expression:

$$l_{0.1} = \frac{1{,}02K_F + 0{,}06}{\frac{K_F}{\cos\varphi} - 0{,}718K_F + 0{,}477K_F^2}. \qquad (14)$$

Thus, the above approximate relations make it possible to optimize the frontal configuration, i.e., to find the optimum values of K_F and ϕ at which, for the specified pressure loss, the rate of mass transfer will be maximal, i.e., the length $\ell_{0.1}$ will be minimal.

NOTATION

z, r, axial and radial coordinates; U_z, U_θ, U_r, axial, tangential, and radial components of velocity, respectively; H, height of the annular channel; B, height of stabilizer; K_F, degree of obstruction; ϕ, angle of opposite swirling of the jets; k, turbulence energy; W, pseudovorticity; $\sqrt{\overline{u}^2}/U_0$, turbulence intensity; L, length of the separation zone; ξ, total pressure loss coefficient; $\ell_{0.1}$, characteristic distance over which the nonuniformity of the concentration profile of the passive impurity decreases to 0.1.

LITERATURE CITED

1. A. G. Tumanovskii, A. V. Sudarev, V. A. Maev, et al., Teploénergetika, No. 3, 37-41 (1986).
2. A. L. Dorfman and V. A. Maev, Inzh.-Fiz. Zh., 41, No. 4, 674-677 (1981).
3. A. A. Sviridenkov, V. V. Tret'yakov, and V. I. Yagodkin, Inzh.-Fiz. Zh., 41, No. 3, 407-413 (1981).
4. T. Vu and G. Guoldin, AIAA Paper, No. 76 (1980).
5. É. D. Sergievskii, A. G. Tumanovskii, K. Yu. Sokolov, et al., Tr. Mosk. Énerg. Inst., No. 78, 98-103 (1985).
6. K. T. Narinder and R. Chevray, J. Fluid Mech., 71, No. 4, 785-800 (1975).
7. J. O. Hunze, Turbulence, McGraw-Hill (1970).
8. I. O. Ilegbusi and D. B. Spalding, Teploperedacha, 107, No. 1, 56-64 (1985).
9. M. L. Koosilin, B. E. Lounder, and B. I. Sharma, Trans. ASEM Ser. C., 96, No. 2, 301-321 (1974).
10. D. B. Spalding, Int. J. Num. Meth. Eng., No. 4, 551-559 (1972).
11. A. I. Maiorova, Inzh.-Fiz. Zh., 46, No. 1, 24-30 (1984).
12. G. N. Abramovich, Theory of Turbulent Jets [in Russian], Moscow (1986).
13. A. V. Sudarev and V. A. Maev, Inzh.-Fiz. Zh., 23, No. 2, 322-327 (1972).